Hindawi Publishing Corporation
Advances in Condensed Matter Physics
Volume 2015, Article ID 920805, 6 pages
http://dx.doi.org/10.1155/2015/920805

Research Article

Photoelectric Characteristics of Double Barrier Quantum Dots-Quantum Well Photodetector

M. J. Wang, F. Y. Yue, and F. M. Guo

Shanghai Key Laboratory of Multidimensional Information Processing, Key Laboratory of Polar Materials & Devices, School of Information Science Technology, East China Normal University, No. 500, Dong Chuan Road, Shanghai 200241, China

Correspondence should be addressed to F. M. Guo; fmguo@ee.ecnu.edu.cn

Received 26 November 2014; Accepted 6 January 2015

Academic Editor: Wen Lei

The photodetector based on double barrier AlAs/GaAs/AlAs heterostructures and a layer self-assembled InAs quantum dots and $In_{0.15}Ga_{0.85}As$ quantum well (QW) hybrid structure is demonstrated. The detection sensitivity and detection ability under weak illuminations have been proved. The dark current of the device can remain at 0.1 pA at 100 K, even lower to 3.05×10^{-15} A, at bias of −1.35 V. Its current responsivity can reach about 6.8×10^5 A/W when 1 pw 633 nm light power and −4 V bias are added. Meanwhile a peculiar amplitude quantum oscillation characteristic is observed in testing. A simple model is used to qualitatively describe. The results demonstrate that the InAs monolayer can effectively absorb photons and the double barrier hybrid structure with quantum dots in well can be used for low-light-level detection.

1. Introduction

Low dimensional nano-scaled III-V semiconductor is a promising candidate material for future high-performance electronics and optoelectronics, including high-mobility field-effect transistors (FETs), long-wavelength infrared photodetectors, and phototransistors [1–5]. Currently, there is great interest in exploring highly sensitive photodetector for potential applications in remote sensing, spectroscopy, and even air quality monitoring in industrial or medical and pro-environment detection. In order to approach the photon counting mode, the very high photoexcited carrier multiplication factor is a basic requirement [6, 7]. Recently, it has been demonstrated that resonant tunneling structure containing a layer of self-assembled quantum dots (QDs) may be used as a very high photoexcited carrier multiplication for low-light-level detection [8–12].

In the present work we discuss peculiar photoelectric conversion characteristics in the double AlAs barrier, self-assembled InAs QDs, and $In_{0.15}Ga_{0.85}As$ QW hybrid structure. When the detector is illuminated with an energy which exceeds GaAs band gap, the photoexcited electrons and holes are generated in the undoped GaAs layers on each side of two AlAs barriers. The photoexcited electrons drift or tunnel by bias toward the lower potential energy and eventually would be captured by the $In_{0.15}Ga_{0.85}As$ QW. The similar process also occur to holes, except that holes drift on the opposite direction and are trapped in the InAs QDs. Due to the spatial separation of electrons and holes, as well as the additional in-plane localization provided by the QDs, the excess electrons and holes could be stored for enough long time. These photovoltaic effects in the wide GaAs quantum well should have each imprint on the photoelectric response. The electrons and holes trapped separately within the $In_{0.15}Ga_{0.85}As$ QW and InAs QDs induce a potential which affects the tunneling characteristics [9, 10]. We can see that the trapped charge strongly affects the tunnel current of the detector which allows for the weak light detection.

The larger current oscillations appear when the detector is illuminated with a 633 nm He-Ne laser under certain conditions. It originates from quantized ballistic motion of photoexcited carriers and is qualitatively different from RTD [3–10]. More than dozens of resonant peaks reveal regions of negative differential conductance in the photocurrent as bias changed from −2 V to 2.5 V and about 100 K temperature. The quantum oscillation appears with typical peak-to-peak voltage interval $\Delta V_{pp} \approx 100$ mV. The electron (and hole) energy levels confined with high quantum numbers successively

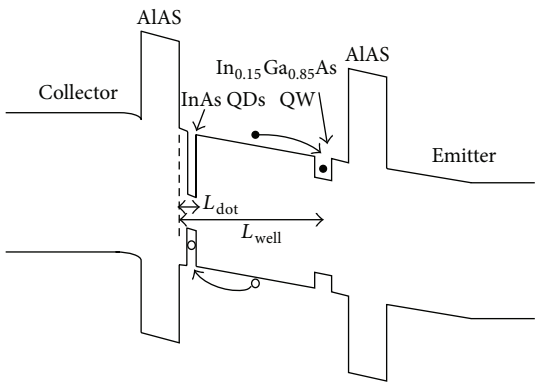

FIGURE 1: Schematic diagram of the capturing of an electron and hole photoexcited in a QW and QD under bias.

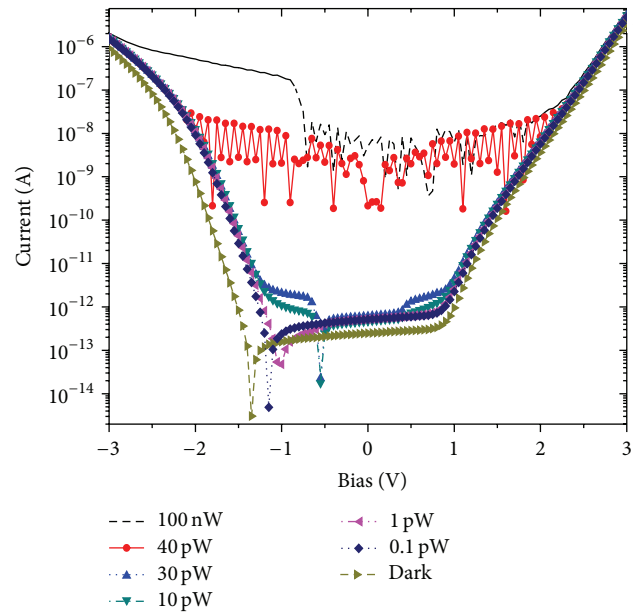

FIGURE 2: The I-V curves at different illumination power.

reach the top of the triangular potential as electric field increased. It causes the tails of the Airy-type wave functions near the classical turning point of the potential to overlap strongly with the high density of free majority carriers in the nearby n doped electrodes. The enhancement of the recombination rate leads to a modulation of the photocurrent measured as a function of applied bias. A model is constructed based on methods of mathematical physics to explain the photocurrent oscillations [10–12].

2. Device Test

The photodetector was grown by MBE on an n^+-type (1 0 0) GaAs substrate; a typical layer structure consists of a 1 μm thick Si-doped (10^{18} cm^{-3}) GaAs buffer layer at the bottom, an undoped 30 nm GaAs spacer, a 25 nm AlAs barrier, a 3 nm GaAs interlayer, a 6 nm $In_{0.15}Ga_{0.85}As$ QW, a 45 nm GaAs wide well, 1.8 ML self-assembled InAs QD layer, a 5 nm GaAs overlayer, and the second 25 nm AlAs barrier. On the top, 30 nm undoped GaAs and 30 nm Si-doped (10^{18} cm^{-3}) GaAs were deposited as the capping layer. Ohmic contacts were made both on the top and at the bottom of the detector meanwhile. A rectangular aperture (50×500 μm^2) was left on the top surface for optical access [10, 13]. The band diagram profile of the detector along its epitaxial growth direction is shown in Figure 1.

The 633 nm He-Ne laser beam with 50 μm diameter was focused on the photosensitive window of the detector. When the bias is at ±1.7 V, the electric field reaches 1×10^7 V/m and the photoexcited electrons and holes are generated in the undoped GaAs layers on each side of the AlAs barriers. The photocurrent-voltage curves of the detector can be recorded by Keithley 4200-SCS. Figure 2 shows the I-V characteristics at incidence light power changing from 0.1 picowatt (pW) to 100 nanowatt (nW). When the bias voltages range from below +1 V to −1.5 V reverse biases, the dark current remains 0.1 pA although the active area is very large (50×500 μm^2). When the detector is biased at −1.35 V, the minimum dark current is only 3.05×10^{-15} A. We can still see when the light power exceeds 40 pW, the oscillatory photocurrent occurs at bias voltages ranging from −2 V to 2.5 V. The oscillatory amplitude also decreases substantially when the bias exceeds 2.5 V or is lower than −2 V. The oscillatory characteristic disappears when light power decreases lower than 40 pW and exceeds 100 nW at bias voltage of −0.6 V.

We can see a reverse bias current valley shifted which changed with illumination power as shown in Figure 2. And the valley shifted more evident as stronger illumination. It represents that the photoexcited holes trapped in the QDs lead to the energy bands downward shift localized, such that a lower bias is required for the detector to reach the large tunneling current [1–7].

Figure 3 shows the higher responsivity of the detector at low-light-level illumination. The current responsivity is larger than 6.8×10^5 A/W when 633 nm light power with 1 pw at −3 V bias is employed. Because an idea quantum efficiency $\eta = 1$, the spectral response $R_{\lambda=633\,\mathrm{nm}}$ is expected to be 0.51 A/W according to [14]

$$\eta = \frac{I_p/e}{P/h\nu} = \frac{Ihc}{gPe\lambda} = \frac{R}{g}\frac{hc}{e\lambda} = \frac{R}{g}\frac{1.24}{\lambda\,(\mu\mathrm{m})}. \quad (1)$$

The gain of the detector can be estimated at least 1.3×10^6. Further, the ratio of the photocurrent versus the dark current can be calculated as shown in Figure 3. When the detector is biased at −1.35 V, the minimum dark current can be gained and then the magnitude of the photocurrent versus the dark current is the largest at this moment.

Figure 4 plots the photocurrent spectra of the detector at 77 K using Bruker FITR Vertex 80 V. The detector shows a good response in the spectral range from 550 nm up to over 930 nm. The photocurrent peak at 818 nm is from the GaAs bulk layer, while the peaks at 873 nm and 925 nm should be attributed to the $In_{0.15}Ga_{0.85}As$ QW and InAs QDs. By the photocurrent spectra, we estimated that the current responsivity at ~925 nm is dozen times more than 633 nm and

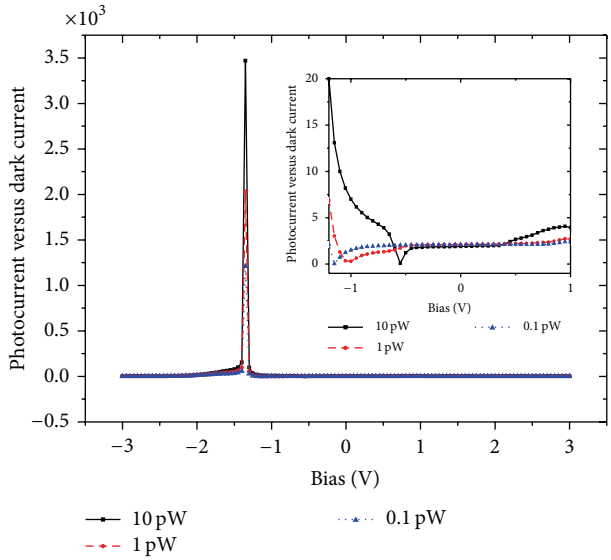

FIGURE 3: Ratio of the photocurrent versus dark current at illumination 55 pw and bias changed from −3 V to 3 V. The inset shows the enlargement of section bias range from −1.2 V to 1 V.

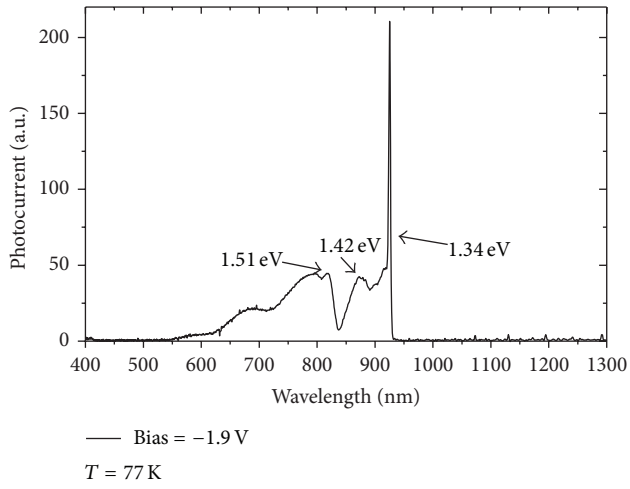

FIGURE 4: Representative photocurrent spectrum of the detector at $T = 77$ K.

thus potentially provides even higher sensitivity. The result indicates that it is a promising detector for sensitive visible to near-infrared imaging applications.

3. Analysis

3.1. Sensitivity. According to Figure 1, a simple model is presented for the detector with one layer of InAs QDs and thin $In_{0.15}Ga_{0.85}As$ QW embedded at distances L_{dot} and L_{well} from one side of AlAs barrier. The QDs layer width is neglectful for simplicity, such that QDs spatial distribution and narrow QW can be modeled by means of a delta function. Poisson's equation with the boundary conditions is as follows [15, 16]:

$$\frac{d^2\varphi}{dx^2} = -\frac{eN_d}{\varepsilon\varepsilon_0} - \frac{ep_{dot}}{\varepsilon\varepsilon_0}\delta\left(x - L_{dot}\right) + \frac{en_{well}}{\varepsilon\varepsilon_0}\delta\left(x - L_{well}\right), \tag{2}$$

$$\varphi\left(w\right) = 0, \tag{3}$$

$$\left.\frac{d\varphi}{dx}\right|_{x=w} = 0. \tag{4}$$

The charge density in the right-hand side of Poisson's equation consists of three components: N_d is the constant charge density of ionized impurity; p_{dot} and n_{well} are the charge density accumulating in QDs and $In_{0.15}Ga_{0.85}As$ QW, respectively. The solution of (2) can be obtained by boundary conditions shown in (3) and (4):

$$\varphi\left(x\right) \approx -\frac{eN_d}{\varepsilon\varepsilon_0}\left(x - w\right)^2 + \begin{cases} 0, & x > L_{well}, \\ -\dfrac{en_{dot}}{\varepsilon\varepsilon_0}\left(L_{dot} - x\right), & x < L_{dot}, \\ \dfrac{en_{dot}}{\varepsilon\varepsilon_0}\left(L_{well} - x\right), & L_{dot} < x < L_{well}. \end{cases} \tag{5}$$

At a larger negative bias, the photoexcited electrons will drift or tunnel toward the side of the lower potential energy and eventually would be captured by the $In_{0.15}Ga_{0.85}As$ QW. The photoexcited holes will drift on opposite direction and be trapped in the InAs QDs. At weak illumination, the QDs and QW layer make little effect on the potential profile because of the very low p_{dot} and n_{well}. As the laser intensity increases, the photoexcited electron-hole pair increases, which means p_{dot} and n_{well} become larger, and induces ΔV photovoltaic effect near the dots, as $x = 0$:

$$\Delta V \approx -\frac{ep_{dot}}{\varepsilon\varepsilon_0}L_{dot}. \tag{6}$$

As the negative bias decreases, the InAs dots capture more holes and the potential near the dots is pulled down gradually. The $In_{0.15}Ga_{0.85}As$ QW captures more electrons and the potential near the QW is pulled up. Such a large ΔV is enough to increase voltage drop of AlAs barrier. That will influence the tunneling process through the AlAs barrier. The higher photosensitivity of the detector indicates a long dwell time of a photoexcited hole following capture at one of the dots. Under appropriate bias voltage, the average electric field in the active region (120 nm wide) of the detector is 10^7 V/cm. Assuming that the mobility of electron and hole is 8000 cm^2/V·s and 400 cm^2/V·s, respectively, their transit times are correspondingly about 1×10^{-14} s and 1×10^{-13} s, which is on a much shorter time than the electron-hole recombination time of about 1×10^{-9} s [10, 15, 16]. Since the transition time is about four orders of magnitude shorter than the electron-hole recombination time, it allows a very high multiplication in detector. At a larger positive bias, the photoexcited electrons will be captured by the InAs QDs and

the photoexcited holes will drift on the opposite direction and be trapped in the $In_{0.15}Ga_{0.85}As$ QW.

For stronger confined ability of QDs compared to QW, the InAs dots capture more holes at negative bias than $In_{0.15}Ga_{0.85}As$ QW at positive bias, and it can get higher detector responsivity in reverse bias.

3.2. Current Oscillations. Under lower level photoexcitation, the space charge density induced by the photoexcited carriers is relatively small. We assume a constant electric field F_z in the intrinsic regions on each side of the barrier layer. We can model for carrier quantization in the formed potential wells by using analytical solutions of the Schrödinger equation at an infinite triangular quantum well. The quantization energies E_j and eigenfunctions $\psi_j(z)$ due to the z component of the carrier motions are given by [12]

$$-\left[\frac{\hbar^2}{2m_e^*}\frac{\partial^2}{\partial z^2}+V(z)\right]\psi(z)=E\psi(Z). \tag{7}$$

The photoexcited electrons occupy the quantized energy subbands j of the triangular potential well. They are influenced by low dimensional quantum effects. The energy of carriers in each subband is given by [12]

$$E_j=\left(\frac{\hbar^2}{2m^*}\right)^{1/3}\left[\frac{3}{2}\pi qF_s\left(j+\frac{3}{4}\right)\right]^{2/3},\quad j=0,1,2,\ldots. \tag{8}$$

The eigenfunctions $\psi_j(z)$ are given by Airy functions:

$$\psi_j(z)=Ai\left[\frac{2m^*qF_z}{\hbar^2}\left(z-\frac{E_j}{qF_z}\right)\right]. \tag{9}$$

Energy level spacing of carriers in each subband is given by

$$\Delta E_j\approx\left(\frac{\hbar}{2m^*}\right)^{1/3}\left[\frac{3}{2}\pi qF_s\left(j+\frac{3}{4}\right)\right]^{-1/3}\pi qF_z. \tag{10}$$

At appropriate bias voltage, an excited state subband with quantum number j_m and energy E_{jm} reaches the top of the triangular quantum well and joins the continuum state of extended electrons above (and below) the conduction (and valence) band edge in the doped electrodes. The voltage interval $V_j - V_{j+1}$, over successive $(j+1)$th and jth levels, reaches the ionization energy, and it can then be estimated and compared with the measured voltage interval ΔV_{pp} between the peaks of the photocurrent.

As electric field F_z increasing, the Airy function state j of a particular hole approaches the top of its triangular potential well and its wave function increasingly overlaps with the high density of majority electrons in the doped n-GaAs electrode. The overlap increases the recombination rate of the photoexcited holes in the j_mth subband, thus reducing their contribution to the photocurrent by tunneling through the AlAs barrier. As the voltage varies, successive Airy function energy levels approach the top of the triangular potential well and join a continuum state of extending the unbounded states in the GaAs conduction band. Hence the competition between tunneling and the bias-dependent modulation of the recombination rate repeats itself, which gives rise to the observed oscillatory photocurrent [12, 17–20].

In addition, the detector may be analogous to N-I-N structure. The photoexcited electrons overlap between the tails of their wave functions and the minority holes in the n-doped layers are very small. The electrons recombination rate with minority holes in the n-GaAs layer is too low to modulate the photocurrent.

As the light power decreases lower than 40 pW as shown in Figure 2, the space charge density induced by the carrier density photoexcited is very small. The recombination current is too low to modulate the photocurrent. This leads to no observation of photocurrent oscillations.

As photoexcitation range changed from 40 pW to 100 nW, the oscillatory amplitude decreases evidently when bias voltage exceeds 2.5 V or becomes lower than −2 V. At higher bias the highest energy states in the triangular potential well are no longer confined by the AlAs barrier so the photocurrent increases rapidly. We note that carriers scattering at the heterointerface between the QD and the surrounding AlAs matrix strongly affects the radiative recombination of photoexcited carriers. A possible explanation for the oscillatory effect is that the QD layer gives rise to a scattering potential which enhances the elastic scattering-assisted tunneling [12].

It is also interesting to note that photocurrent oscillates at bias voltages that range from −0.6 V to 2.5 V and disappears at −0.6 V negative bias whose higher photoexcitation state is ~100 nW. The photoexcited electron-hole pairs induce larger ΔV photovoltaic changed, so the tunneling current increases rapidly and the recombination current is too low to modulate the photocurrent.

4. 64-Pixel Line Readout

To read out the weak light response, a 1 × 64 array readout circuit and an on-chip integrated system for data processing with low noise and high precision are designed. Figure 5 is the readout response voltage of the 64-pixel line with laser beam power at ~1 nw, the integration time 29 μs, and indoor temperature. Due to the working point of inconsistencies for some pixels, their readout voltage is saturated and premature. The inset shows the response voltage of the most normal pixel. The response voltage is changed in approximate linear when the light power changed from 10 pw to 100 pw. The response voltage is 27 mV at 10 pw illumination beam power and 35 μs integration time. The voltage responsivity reaches about 2.7×10^9 V/W.

5. Conclusion

We have measured and analyzed the photoelectric characteristics of the AlAs/GaAs/AlAs double barrier structure photodetector, which contains a layer of self-assembled InAs QD and thin $In_{0.15}Ga_{0.85}As$ QW in AlAs double barriers. The higher sensitivity is caused by the charge effect of the photoexcited holes and electrons captured by surrounding

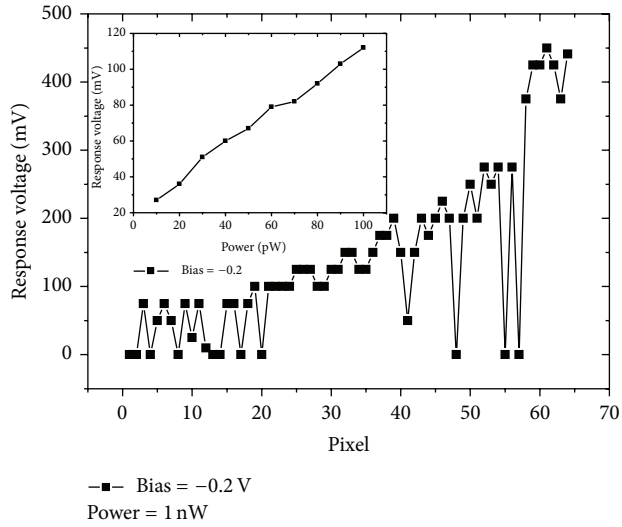

Figure 5: Readout voltage of the 64-pixel linear array at 1 nW illuminated beam (633 nm) power. The inset shows the 61th pixel response voltage at indoor temperature and laser (633 nm) power changed from 10 pw to 100 pw.

QDs and $In_{0.15}Ga_{0.85}As$ QW, respectively. The oscillations appear when the detector is illuminated with 633 nm He-Ne laser beam at certain bias and incidence. The competition between tunneling and the bias-dependent modulation of the recombination rate repeats itself giving rise to the oscillatory photocurrent observed. Further, we find the photocurrent tails up to 930 nm wavelength with high sensitivity. The readout results demonstrate that the photodetector shows good sensitivity when light power (633 nm) is as low as 10 pW at indoor temperature.

Conflict of Interests

The authors declare that there is no conflict of interests regarding the publication of this paper.

Acknowledgments

This work was supported by the National Scientific Research Plan (2011CB932903), the Scientific and Technological Commission of Shanghai (no. 118014546), the Natural Science Foundation of China (61376103), the State Key Laboratory of Functional Materials for Informatics, and Laboratory for Terahertz Solid State Technology Chinese Academy of Science.

References

[1] E. E. Vdovin, A. Levin, A. Patane et al., "Imaging the electron wave function in self-assembled quantum dots," *Science*, vol. 290, no. 5489, pp. 122–124, 2000.

[2] J. C. Blakesley, P. See, A. J. Shields et al., "Efficient single photon detection by quantum dot resonant tunneling diodes," *Physical Review Letters*, vol. 94, no. 6, Article ID 067401, 2005.

[3] S. S. Hees, B. E. Kardynal, P. See, A. J. Shields, I. Farrer, and D. A. Ritchie, "Effect of InAs dots on noise of quantum dot resonant tunneling single-photon detectors," *Applied Physics Letters*, vol. 89, no. 15, Article ID 153510, 3 pages, 2006.

[4] N. Guo, W. Hu, L. Liao et al., "Anomalous and highly efficient InAs nanowire phototransistors based on majority carrier transport at room temperature," *Advanced Materials*, vol. 26, no. 48, pp. 8203–8209, 2014.

[5] J. Miao, W. Hu, N. Guo et al., "Single InAs nanowire room-temperature near-infrared photodetectors," *ACS Nano*, vol. 8, no. 4, pp. 3628–3635, 2014.

[6] W. Lu, Y. M. Mu, X. Q. Liu et al., "Direct observation of above-quantum-step quasibound states in GaAs/AlxGa1-xAs/vacuum heterostructures," *Physical Review B—Condensed Matter and Materials Physics*, vol. 57, no. 16, pp. 9787–9791, 1998.

[7] W. Wang, Y. Hou, D. Xiong et al., "High photoexcited carrier multiplication by charged InAs dots in AlAs/GaAs/AlAs resonant tunneling diode," *Applied Physics Letters*, vol. 92, no. 2, Article ID 023508, 2008.

[8] Q. C. Weng, Z. H. An, D. Y. Xiong et al., "Photocurrent spectrum study of a quantum dot single-photon detector based on resonant tunneling effect with near-infrared response," *Applied Physics Letters*, vol. 105, no. 3, Article ID 031114, 3 pages, 2014.

[9] T. M. Fromhold, L. Eaves, F. W. Sheard, M. L. Leadbeater, T. J. Foster, and P. C. Main, "Magnetotunneling spectroscopy of a quantum well in the regime of classical chaos," *Physical Review Letters*, vol. 72, no. 16, pp. 2608–2611, 1994.

[10] B. Hu, X. Zhou, Y. Tang et al., "Photocurrent response in a double barrier structure with quantum dots-quantum well inserted in central well," *Physica E: Low-Dimensional Systems and Nanostructures*, vol. 33, no. 2, pp. 355–358, 2006.

[11] J. Wen, L. Li, Q. C. Weng, and D. Y. Xiong, "Simulation of resonant tunneling devices: origin of the $I - V$ multi-peak behavior," *Optical and Quantum Electronics*, vol. 45, no. 7, pp. 783–790, 2013.

[12] E. E. Vdovin, M. Ashdown, A. Patanè et al., "Quantum oscillations in the photocurrent of GaAs/AlAs p-i-n diodes," *Physical Review B—Condensed Matter and Materials Physics*, vol. 89, no. 20, Article ID 205305, 2014.

[13] H.-Z. Zheng, H.-F. Li, Y.-M. Zhang et al., "Experimental study of tunneling escape through double-barrier resonant-tunneling structures," *Physical Review B*, vol. 51, no. 16, pp. 11128–11131, 1995.

[14] F. Hartmann, F. Langer, D. Bisping et al., "GaAs/AlGaAs resonant tunneling diodes with a GaInNAs absorption layer for telecommunication light sensing," *Applied Physics Letters*, vol. 100, no. 17, Article ID 172113, 3 pages, 2012.

[15] A. J. Chiquito, Y. A. Pusep, S. Mergulhão, J. C. Galzerani, and N. T. Moshegov, "Effect of photogenerated holes on capacitance-voltage measurements in InAs/GaAs self-assembled quantum dots," *Physical Review B: Condensed Matter and Materials Physics*, vol. 61, no. 7, pp. 4481–4484, 2000.

[16] S. D. Lin, V. V. Ilchenko, V. V. Marin et al., "Observation of the negative differential capacitance in Schottky diodes with InAs quantum dots near room temperature," *Applied Physics Letters*, vol. 90, no. 26, Article ID 263114, 3 pages, 2007.

[17] M. Narihiro, G. Yusa, Y. Nakamura, T. Noda, and H. Sakaki, "Resonant tunneling of electrons via 20 nm scale InAs quantum dot and magnetotunneling spectroscopy of its electronic states," *Applied Physics Letters*, vol. 70, no. 1, pp. 105–107, 1997.

[18] O. Makarovsky, E. E. Vdovin, A. Patané et al., "Laser location and manipulation of a single quantum tunneling channel in an InAs quantum dot," *Physical Review Letters*, vol. 108, no. 11, Article ID 117402, 2012.

[19] G. R. Li, X. Zhou, F. H. Yang, P. H. Tan, H. Z. Zheng, and Y. P. Zeng, "Photo-capacitance response of internal tunnelling coupling in quantum-dot-imbedded heterostructures under selective photo-excitation," *Journal of Physics Condensed Matter*, vol. 16, no. 36, pp. 6519–6525, 2004.

[20] Y. Tang, H. Zheng, F. Yang, P. Tan, C. Li, and Y. Li, "Electrical manifestation of the quantum-confined Stark effect by quantum capacitance response in an optically excited quantum well," *Physical Review B*, vol. 63, no. 11, Article ID 113305, 4 pages, 2001.